Acta Crystallographica Section A
Foundations of Crystallography
ISSN 0108-7673

Received 8 February 2010
Accepted 18 April 2010

Multipole electron-density modelling of synchrotron powder diffraction data: the case of diamond

H. Svendsen,[a] J. Overgaard,[a] R. Busselez,[b] B. Arnaud,[b] P. Rabiller,[b] A. Kurita,[c] E. Nishibori,[c] M. Sakata,[c] M. Takata[d] and B. B. Iversen[a]*

[a]Center for Materials Crystallography, Department of Chemistry and iNANO, Aarhus University, DK-8000 Aarhus C, Denmark, [b]Institut de Physique de Rennes, Université de Rennes 1, UMR CNRS 6626, Rennes 35042, France, [c]Department of Applied Physics, Nagoya University, Furo-cho, Chikusa, Nagoya 464-8603, Japan, and [d]SPring8 Synchrotron, Koto 1-1-1, Sayo-cho, Sayo, Hyougo 679-5148, Japan. Correspondence e-mail: bo@chem.au.dk

Accurate structure factors are extracted from synchrotron powder diffraction data measured on crystalline diamond based on a novel multipole model division of overlapping reflection intensities. The approach limits the spherical-atom bias in structure factors extracted from overlapping powder data using conventional spherical-atom Rietveld refinement. The structure factors are subsequently used for multipole electron-density modelling, and both the structure factors and the derived density are compared with results from *ab initio* theoretical calculations. Overall, excellent agreement is obtained between experiment and theory, and the study therefore demonstrates that synchrotron powder diffraction can indeed provide accurate structure-factor values based on data measured in minutes with limited sample preparation. Thus, potential systematic errors such as extinction and twinning commonly encountered in single-crystal studies of small-unit-cell inorganic structures can be overcome with synchrotron powder diffraction. It is shown that the standard Hansen–Coppens multipole model is not flexible enough to fit the static theoretical structure factors, whereas fitting of thermally smeared structure factors has much lower residuals. If thermally smeared structure factors (experimental or theoretical) are fitted with a slightly wrong radial model (s^2p^2 instead of sp^3) the radial scaling parameters ('κ' parameters) are found to be inadequate and the 'error' is absorbed into the atomic displacement parameter. This directly exposes a correlation between electron density and thermal parameters even for a light atom such as carbon, and it also underlines that in organic systems proper deconvolution of thermal motion is important for obtaining correct static electron densities.

1. Introduction

The determination of electron-density distributions (EDDs) from X-ray diffraction data is a vibrant field of modern crystallography (Tsirelson & Ozerov, 1996; Coppens, 1997; Koritsansky & Coppens, 2001; Coppens *et al.*, 2005). The overwhelming majority of studies use aspherical density models centred on the atomic positions to describe the static EDD of the unit cell (multipole model) and the parameters of the model are estimated by the least-squares method (Stewart, 1976; Hansen & Coppens, 1978). Since the multipole model requires many (subtle) parameters, which also must separate the thermal-motion effects from the static aspherical density effects, the X-ray data quality is imperative in these studies. Not only must the X-ray structure factors be both accurate and precise, they must also be very abundant to allow robust least-squares estimates of the many parameters. Experimentally there has been much effort to minimize various systematic errors in the data such as absorption, extinction, anomalous scattering, anharmonicity, scan truncation, thermal diffuse scattering *etc.* (Iversen *et al.*, 1996, 1999). Major advances have occurred with the availability of short-wavelength, high-intensity synchrotron radiation, quick and reliable area detectors [CCDs (charge-coupled devices), image plates] and stable helium-based cooling devices (Bolotovsky *et al.*, 1995; Koritsanszky *et al.*, 1998; Overgaard *et al.*, 2001, 2002, 2003; Poulsen *et al.*, 2005; Clausen *et al.*, 2008; Morgenroth *et al.*, 2008).

It is generally believed that single-crystal data are more accurate than powder data due to the inherent problems of

extracting individual structure factors from overlapping powder diffraction reflections. While this is probably true in many cases, it is not necessarily so for high-symmetry inorganic crystal structures. On the contrary, in these systems extinction effects can be severe in the low-order single-crystal data due to a high degree of crystal perfection and twinning may be difficult to avoid. Furthermore, powder data can be measured in a single image, making the scale of the different reflections identical. Sakata, Takata and co-workers developed a way to obtain maximum-entropy method (MEM) electron densities from structure factors (Sakata & Sato, 1990; Kumazawa *et al.*, 1993; Iversen *et al.*, 1995; Roversi *et al.*, 1998). When synchrotron powder diffraction data are employed the method uses an iterative approach of cyclic Rietveld and MEM calculations to obtain a grid representation of the thermally smeared electron density (Takata *et al.*, 1995). The method has provided important results in many chemical and physical studies (Takata *et al.*, 2001; Kitaura *et al.*, 2002), but it has been limited by difficulties in quantitative interpretation of the thermally smeared densities. Interpretation within the quantum theory of atoms in molecules to some extent overcomes this limitation (Iversen *et al.*, 1995; Cargnoni *et al.*, 2004; Hofmann *et al.*, 2007; van Smaalen & Netzel, 2009), but parameterization of static electron-density features as well as thermal motion (*i.e.* the multipole model) is still desirable in many cases (*e.g.* in comparisons with theoretical results). In the Rietveld/MEM approach the powder data are first analysed by Rietveld whole-pattern fitting (Takata *et al.*, 2001). The Rietveld programs use a spherical independent atom model (IAM) to describe the static EDD, as well as parameters modelling the thermal motion, the background, the peak shape *etc.* When individual structure factors are extracted from the observed intensities of overlapping reflections, the individual contributions from each structure factor to a measured data point are estimated from the IAM. This inevitably introduces an 'atomic bias' in the extracted structure-factor values. However, since peak overlap is only a problem at higher order, the low-order structure factors containing the majority of the bonding features should be well determined even with an IAM model. This is one reason for the success of the many Rietveld/MEM studies in showing accurate aspherical bonding features. Furthermore, for spherical-atom systems, such as heavy-atom ionic structures, this atomic bias is limited. In such structures inadequate division of overlapping reflections could come from deficiencies in the thermal motion (anharmonicity), which makes it important to conduct the studies at the lowest possible temperature.

Here we explore the spherical-atom bias in the Rietveld method by extracting structure factors from short-wavelength, very high resolution synchrotron powder diffraction data. As a test example we use crystalline diamond, which is an example of a covalent network structure, where aspherical bonding effects are expected to be substantial even though the unit cell is small, limiting peak overlap at low angles. Since we are not aware of any powder analysis programs employing multipole models in the Rietveld refinement, we have chosen an iterative scheme based on the widely used multipole modelling program *XD* (Volkov *et al.*, 2006) in combination with a standard IAM Rietveld program *SP* (Nishibori *et al.*, 2007). We use the multipole-model-extracted powder diffraction structure factors for multipole modelling of the electron density, and the results are compared with *ab initio* theoretical results.

The electron density of diamond has been investigated numerous times before by both theory and experiments. Several different charge-density models have been used to analyse the conventional X-ray powder data of Göttlicher & Wölfel (1959), which were measured to a resolution of 1.28 Å^{-1} (Weiss, 1964; Dawson, 1967; Dawson & Sanger, 1967; McConnell & Sanger, 1970; Kurki-Suonio & Ruuskanen, 1971; Stewart, 1973*a*,*b*; Harel *et al.*, 1975; Price & Maslen, 1978). Highly accurate structure factors have also been measured by the *Pendellösung* method to 0.79 Å^{-1} (Takama *et al.*, 1990) and these data have been analysed by Spackman (1991) and Yamamoto *et al.* (1996). For comparison, the present synchrotron powder diffraction data have a maximum $\sin\theta/\lambda$ of 1.45 Å^{-1}.

Our study also serves another purpose. In the literature there has been much discussion about the applicability of the X-ray method for determination of experimental electron densities in small-unit-cell inorganic solids (Zuo *et al.*, 1999; Wang & Schwarz, 2000; Schwarz, 2006). It has been argued that convergent-beam electron diffraction is the method of choice for such compounds, in particular due to postulated 'unavoidable' extinction effects in the critical low-order structure factors. It is exactly in the important low-order reflections containing most of the valence information that electron diffraction is argued to be most accurate. Irrespective of these discussions, it is a severe limitation that convergent-beam electron diffraction is a highly specialized and time-consuming technique, where measurement of a few reliable structure factors takes weeks and has severe sample restrictions. Furthermore, such studies must be combined with X-ray studies at matching temperatures to provide a description of the thermal motion, which opens up the possibility of substantial scaling errors. Here we show that accurate struc-

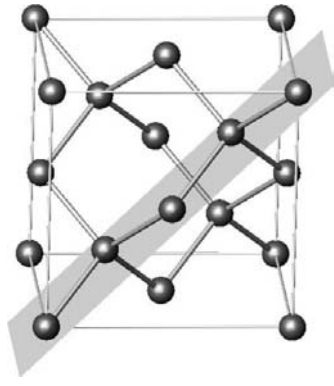

Figure 1
The structure of diamond showing the content of one unit cell translated 1/8 in each direction. A section of the (110) plane is marked indicating the plane used in the electron-density plots.

Table 1
Structure factors for diamond at 100 K up to $\sin\theta/\lambda = 1.45$ Å^{-1} on an absolute scale.

F^{sph} and F^{asph} are observed structure factors extracted using a spherical IAM and an aspherical multipole model, respectively. F^{asph}_{anh} is observed structure factors obtained using an aspherical multipole model together with anharmonic thermal parameters. F^{IAM} and $F^{multipole}$ are calculated model structure factors from *XD* based on a spherical and a multipole refinement of F^{dyn}, respectively. F^{sta} are calculated static structure factors using *ab initio* theory, and F^{dyn} are obtained from F^{sta} by convoluting a thermal parameter of 0.00188 Å^2 on the density.

h k l	F^{sph}	F^{asph}	F^{asph}_{anh}	F^{IAM}	$F^{multipole}$	F^{sta}	F^{dyn}
1 1 1	18.43 (3)	18.46 (3)	18.62 (3)	17.29	18.53	18.67	18.51
2 2 0	15.38 (3)	15.40 (3)	15.53 (3)	15.63	15.49	15.85	15.48
3 1 1	9.21 (3)	9.22 (2)	9.30 (2)	9.80	9.34	9.63	9.33
4 0 0	11.92 (6)	11.91 (5)	12.01 (5)	12.25	11.98	12.54	11.97
3 3 1	8.44 (3)	8.44 (3)	8.51 (3)	8.21	8.39	8.85	8.37
4 2 2	10.78 (4)	10.78 (3)	10.87 (3)	10.76	10.79	11.54	10.76
3 3 3	7.21 (6)	7.14 (6)	7.18 (6)	7.29	7.22	7.78	7.20
5 1 1	7.23 (4)	7.25 (3)	7.32 (3)	7.29	7.29	7.87	7.28
4 4 0	9.72 (5)	9.71 (5)	9.80 (5)	9.64	9.67	10.61	9.67
5 3 1	6.56 (3)	6.56 (3)	6.61 (3)	6.55	6.54	7.25	6.55
6 2 0	8.65 (4)	8.65 (4)	8.72 (4)	8.68	8.69	9.77	8.69
5 3 3	5.99 (4)	5.99 (4)	6.04 (4)	5.91	5.96	6.74	5.94
4 4 4	7.92 (8)	7.92 (7)	7.98 (7)	7.85	7.87	9.05	7.87
5 5 1	5.35 (5)	5.36 (4)	5.40 (4)	5.35	5.37	6.23	5.37
7 1 1	5.35 (5)	5.34 (4)	5.38 (5)	5.35	5.35	6.22	5.36
6 4 2	7.15 (4)	7.15 (3)	7.21 (3)	7.11	7.12	8.40	7.13
5 5 3	4.84 (5)	4.83 (5)	4.88 (5)	4.85	4.85	5.77	4.86
7 3 1	4.86 (4)	4.86 (3)	4.90 (3)	4.85	4.86	5.77	4.86
8 0 0	6.47 (10)	6.47 (10)	6.53 (10)	6.46	6.46	7.80	6.47
7 3 3	4.44 (5)	4.44 (5)	4.48 (5)	4.41	4.41	5.37	4.42
8 2 2	5.88 (5)	5.88 (5)	5.92 (5)	5.88	5.88	7.27	5.89
6 6 0	5.86 (7)	5.85 (7)	5.91 (7)	5.88	5.88	7.27	5.89
5 5 5	3.98 (9)	3.99 (9)	4.01 (9)	4.01	4.02	5.00	4.02
7 5 1	4.01 (4)	4.01 (4)	4.05 (4)	4.01	4.01	5.01	4.02
8 4 0	5.34 (6)	5.33 (5)	5.37 (5)	5.36	5.36	6.78	5.37
7 5 3	3.66 (4)	3.66 (4)	3.69 (4)	3.66	3.67	4.68	3.67
9 1 1	3.66 (5)	3.65 (5)	3.68 (5)	3.66	3.66	4.68	3.67
6 6 4	4.86 (6)	4.85 (6)	4.90 (6)	4.90	4.90	6.35	4.91
9 3 1	3.35 (4)	3.34 (4)	3.37 (4)	3.35	3.35	4.38	3.36
8 4 4	4.49 (6)	4.48 (6)	4.51 (6)	4.49	4.49	5.95	4.50
7 5 5	3.03 (6)	3.02 (6)	3.06 (6)	3.07	3.07	4.11	3.08
7 7 1	3.03 (6)	3.02 (6)	3.04 (6)	3.07	3.07	4.11	3.08
9 3 3	3.03 (6)	3.02 (6)	3.04 (6)	3.07	3.07	4.11	3.08
8 6 2	4.10 (4)	4.09 (4)	4.13 (4)	4.12	4.12	5.60	4.13
10 2 0	4.09 (6)	4.08 (6)	4.11 (6)	4.12	4.11	5.60	4.13
7 7 3	2.77 (6)	2.76 (6)	2.80 (6)	2.82	2.82	3.87	2.83
9 5 1	2.77 (4)	2.77 (4)	2.79 (4)	2.82	2.82	3.87	2.83

ture factors can be extracted from synchrotron powder diffraction data measured in minutes without any difficult sample preparation.

2. Experimental and theoretical details

The synchrotron powder diffraction data for diamond used in the present analysis were recently published by Nishibori *et al.* (2007). The data were collected on the large Debye–Scherrer image-plate camera at beamline BL02B2, SPring8, Japan, and we refer readers to the paper of Nishibori *et al.* (2007) for a detailed discussion of the experimental procedures. Here we note that the data were measured at 100 K using a wavelength of 0.40096 Å up to a maximum of 1.45 Å^{-1} in $\sin\theta/\lambda$. The cubic unit cell of diamond was determined to be 3.5671 (3) Å from Rietveld refinement of the data with the carbon atom at (0.125, 0.125, 0.125) in space group $Fd\bar{3}m$ (see Fig. 1).

Initially, structure factors were extracted from the synchrotron powder diffraction pattern using an IAM in a standard Rietveld refinement approach and the 'conventional IAM' values are listed in Table 1 as F^{sph}. This set of structure factors is referred to as the spherical or IAM-extracted structure factors. Please note that these are *observed* structure factors and that the IAM model has merely been used to divide intensities in case of peak overlap. These structure factors correspond to the values used by Nishibori *et al.* (2007) in their Rietveld/MEM analysis. The F^{sph} structure factors were used as input for multipole electron-density analysis with the program *XD* (Volkov *et al.*, 2006). The multipole refinements were performed using radial functions based on an sp^3 hybridized carbon atom [atom Cv from the SCM scattering data bank in *XD*, which is based on wavefunctions fitted to a relativistic Dirac–Fock solution (Su & Coppens, 1998; Macchi & Coppens, 2001)]. Two independent multipolar functions (O2−, H0) are allowed by symmetry up to fourth order on the carbon atom, while a third hexadecapole H4+ is constrained to H0 by H4+ = (0.74045)H0 (Volkov *et al.*, 2006). The multipole model also refined a scale factor, two radial κ parameters and one harmonic thermal parameter. Refinement of an isotropic extinction parameter gave insignificant values as expected for powder data. Based on this multipole model, thermally smeared structure factors were calculated and these replaced the spherical-atom IAM values used in the Rietveld refinement to extract a new set of structure factors from the experimental data. Thus, in the structure-factor extraction, the observed intensities of overlapping reflections were divided according to the multipole model rather than the IAM model. The new set of structure factors was then fed into the program *XD* for a second multipole refinement. The procedure was continued until no changes were seen in the extracted observed structure factors and these are shown in Table 1 as F^{asph}. All structure factors listed in Table 1 are scaled to absolute values using the scale factor from *XD*. To account for possible errors in the thermal-motion model, which may be important for the high-order data where peak overlap is severe, anharmonic Gram–Charlier parameters were then introduced to fourth order and the iterative structure-factor extraction was continued until convergence for an aspherical electron-density model; these structure factors are listed in Table 1 as F^{asph}_{anh}. The anharmonic

thermal parameters were constrained by $d1111 = d2222 = d3333$ and $d1122 = d1133 = d2233$.

Theoretical structure factors (F^{sta}) were derived from an all-electron density functional theory (DFT) calculation, using the *PAW* code (Blöchl, 1994) within the local density approximation (LDA) and applying Perdew–Burke–Ernzerhof (PBE) gradient corrections (Perdew *et al.*, 1996). A 30 Ry cutoff was applied to the plane-wave expansion and the total electron density was output on a grid with 0.1 atomic unit mesh size. Since there is only one atom in the unit cell of diamond, dynamical theoretical structure factors (F^{dyn}) can be obtained merely by multiplication of F^{sta} with a temperature factor having a given atomic displacement parameter (ADP). This raises the question of what is the best value of the ADP. It is possible to deconvolute the observed structure factors by comparing them with the theoretical static structure factors. A linear least-square fit has been applied to the function $\ln(F^2_{obs}/F^2_{theo}) = \ln(k) - 16\pi^2\langle u^2\rangle[\sin(\theta)/\lambda]^2$ for both the spherical (*i.e.* IAM) and aspherical (*i.e.* multipole) extracted structure factors. The results are plotted in Fig. 2.

The mean square displacements ($\langle u^2\rangle$) are found to be identical within the estimated standard uncertainty, and values of 0.00186 (2) and 0.00188 (2) Å^2 are obtained for the observed structure factors extracted with the spherical and aspherical density models, respectively. Dynamic theoretical structure factors (F^{dyn}) were calculated by convolution of F^{sta} with the thermal parameter determined from the fitting of F^{asph} (0.0188 Å^2). The static and dynamic theoretical structure factors are also listed in Table 1. Multipole refinements of these theoretical structure factor sets have been performed using unit weights. Refinements using the experimentally determined uncertainties have also been performed, but they did not result in significantly different multipole models.

Table 1 also contains calculated model structure factors obtained from a spherical IAM model as well as an aspherical multipole model refinement of F^{dyn} in *XD* using the same thermal parameter ($\langle u^2\rangle$ = 0.00188 Å^2) as used for obtaining dynamic theoretical structure factors (F^{dyn}) from the static theoretical structure factors (F^{sta}). These two sets of model structure factors are denoted F^{IAM} and $F^{multipole}$, respectively. For spherical-atom densities in the harmonic approximation of the thermal motion, the reflection extinction rules do not allow reflections with $h + k + l = 4n + 2$. However, depending on the temperature, non-spherical atoms or anharmonic thermal motion may lead to non-zero intensity in such reflections. Asphericity and anharmonicity are 'opposing' effects and they may cancel each other at some specific temperature (Alkire *et al.*, 1982; Trucano & Batterman, 1972; Tischler & Batterman, 1984). Since the weakly 'forbidden' reflections (222), (442) and (622) are not included in the experimental data sets, these reflections have been removed from the theoretical data to facilitate direct comparison. In the theoretical data the intensity of the (222) reflection is less than 5% of the most intense (111) reflection. If the (222) reflection is included in the refinement, no significant changes are observed in the obtained multipole model.

3. Results and discussion

3.1. Spherical *versus* aspherical structure-factor extraction

In this section we compare the structure factors listed in Table 1 by plotting structure-factor ratios F^1/F^2 *versus* $\sin\theta/\lambda$, calculating ratio averages $\langle F^1/F^2\rangle$ and residual factors $R(F^1, F^2) = \sum(F^1 - F^2)/\sum F^2$. The latter two are listed in Table 2 for various combinations of structure factors, while Fig. 3 shows ratios *versus* $\sin\theta/\lambda$.

A natural benchmark for all the obtained structure-factor sets is to compare them with values calculated for model structure factors F^{IAM} and $F^{multipole}$. Thus, $R(F^{IAM}, F^{multipole}) = 0.0112$ represents the limit of 'atomic bias' in the structure-factor extraction procedure. A value of 1.12% shows that there

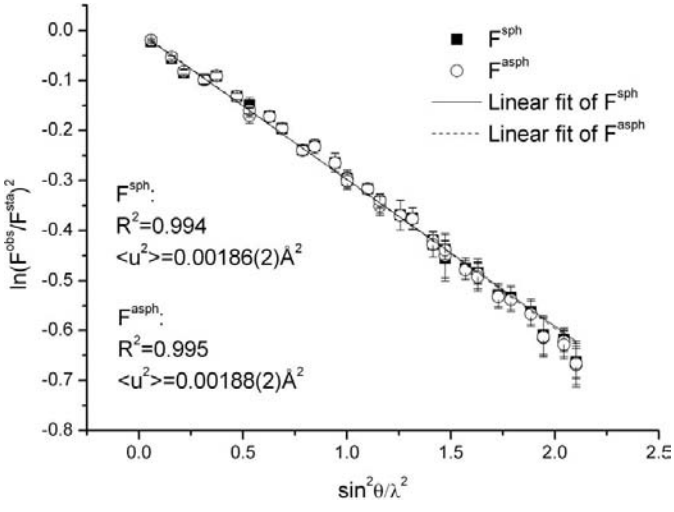

Figure 2
$\ln(F^{asph}/F^{sta})^2$ plotted as function of $\sin^2\theta/\lambda^2$.

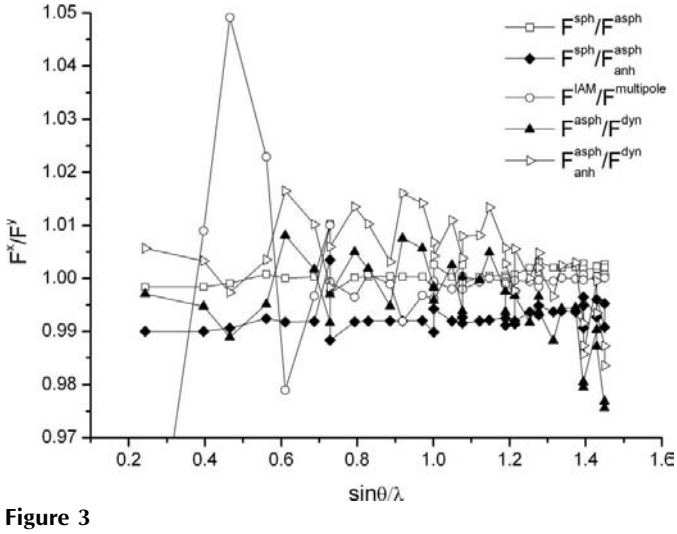

Figure 3
Structure-factor ratios plotted as a function of $\sin\theta/\lambda$. The first point for $F^{IAM}/F^{multipole}$ is at 0.91.

Table 2
Residual factors $R(F^1, F^2) = \sum(F^1 - F^2)/\sum F^2$ and ratio averages $\langle F^1/F^2\rangle$ for various combinations of structure factors.

$R(F^{sph}, F^{asph})$	0.0015	$\langle F^{sph}/F^{asph}\rangle$	1.001
$R(F^{sph}/F^{asph}_{anh})$	0.0079	$\langle F^{sph}/F^{asph}_{anh}\rangle$	0.993
$R(F^{asph}_{anh}, F^{asph})$	0.0084	$\langle F^{asph}/F^{asph}_{anh}\rangle$	1.008
$R(F^{IAM}, F^{multipole})$	0.0112	$\langle F^{IAM}/F^{multipole}\rangle$	0.999
$R(F^{sph}, F^{dyn})$	0.0059	$\langle F^{sph}/F^{dyn}\rangle$	0.995
$R(F^{asph}, F^{dyn})$	0.0062	$\langle F^{asph}/F^{dyn}\rangle$	0.994
$R(F^{asph}_{anh}, F^{dyn})$	0.0069	$\langle F^{asph}_{anh}/F^{dyn}\rangle$	1.003

are small but significant differences between spherical and aspherical model structure factors. The R value for the observed structure factors, $R(F^{sph}, F^{asph}) = 0.0015$, is an order of magnitude lower than the difference between the model structure factors. In Fig. 3 the ratios F^{sph}/F^{asph} and $F^{IAM}/F^{multipole}$ are plotted as a function of $\sin\theta/\lambda$. In diamond the bonds are highly covalent; hence the largest differences are expected in the low-angle region, where the valence electrons dominate. This is exactly what is observed for the $F^{IAM}/F^{multipole}$ ratio but no significant differences are seen in the low-angle region for the observed structure factors extracted using a spherical IAM model and the aspherical multipole model, respectively. The ratio F^{sph}/F^{asph} is almost constant as a function of $\sin\theta/\lambda$ indicating no significant differences between the two structure-factor sets.

The spherical and aspherical structure factors, the latter for both the harmonic and anharmonic refinements, have been compared with theoretical dynamic structure factors. From the ratios and R values between various combinations of these structure factor sets, it can be concluded that the structure factors extracted using harmonic temperature factors are in best agreement with the theoretical structure factors with R values as low as $R(F^{sph}, F^{dyn}) = 0.0059$ and $R(F^{asph}, F^{dyn}) = 0.0062$ compared with 0.0069 for $R(F^{asph}_{anh}, F^{dyn})$. This comparison demonstrates that the atomic bias is limited in the structure-factor extraction due to the relatively modest peak overlap at low order. The intensity of the overlapping peaks is divided between the peaks according to the ratio between the calculated model intensities. In the low-angle region where the differences between the models are largest, only very limited peak overlap is present and the structure factors obtained for diamond are therefore almost independent of the choice of model for extracting observed structure factors. This shows that even if an IAM model is used in the extraction of powder-diffraction structure factors, the aspherical bonding features are still included in these structure factors and the 'atomic bias' is small. It is therefore not surprising that the Rietveld/MEM method based on spherical structure-factor extraction has been used with much success.

From the R values in Table 2, it is seen that the difference between the harmonic and anharmonic aspherical structure factors, $R(F^{asph}, F^{asph}_{anh}) = 0.0084$, is larger than the difference between the spherical and aspherical structure factors, $R(F^{sph}, F^{asph}) = 0.0015$. The larger value of $R(F^{asph}_{anh}, F^{dyn}) = 0.0069$ shows that structure factors extracted with anharmonic parameters in the model have a larger disagreement with the theoretical set (see also Fig. 3). The strong covalent bonds in diamond are an effect of a steep potential well, and indeed diamond has an extremely small thermal expansion. Even though anharmonic effects are present in the diamond-type lattice of silicon at 293 K (Flensburg & Stewart, 1999), it is unlikely that there are measurable anharmonic effects in diamond at 100 K. Diamond is the hardest material in Nature and the Debye temperature is as high as 1860 K compared with 645 K for silicon (Ashcroft & Mermin, 1976). The straight line obtained in the Wilson plot in Fig. 2 confirms that anharmonicity is very limited at 100 K in diamond. In the present case incorporation of 'unphysical' anharmonic thermal parameters has more effect on the structure-factor extraction than including a multipole model for description of the static density. In other words, one should be careful when introducing anharmonic thermal parameters. The thermal motion especially affects the high-angle region, and it is also in this region peak overlap is observed in powder-diffraction data. When anharmonic thermal parameters are introduced in the extraction they have a significant influence on the intensity division between overlapping peaks.

3.2. Multipole refinements

In Table 3 the refined parameters and residuals for different *XD* multipole refinements are listed. Table 4 lists the topological features of the C—C bond critical point for the different refinements. First, it is of interest to carry out a multipole refinement of the static structure factors obtained from *ab initio* theory. In this refinement the thermal parameters are fixed to zero value. This gives a reference for an optimal multipole model with which all refinements of the experimental data set can be compared, *i.e.* it shows to what extent the multipole model can account for the electron density in diamond. The multipole model fits the static structure factors quite well with RF and RF^2 as low as 0.0019 and 0.0028, respectively. However, as can be seen in Table 3 and Fig. 4, the resulting residuals are not zero and the residual density has values in the interval −0.065–0.121 e Å^{-3}. Apparently the bonding density has been fitted by the multipole model but a radial deficiency near the nuclei (spherical 'ring-like' features)

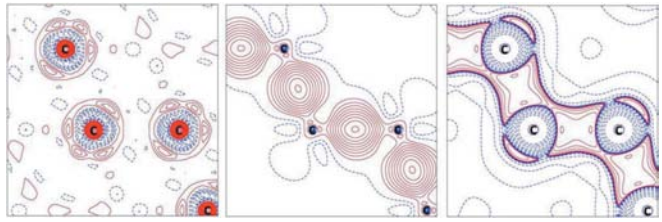

Figure 4
Refinement of F^{sta}. Left is the residual density with contour level 0.01 e Å^{-3}, middle is the static deformation density with contour level 0.05 e Å^{-3}, and right is the negative Laplacian with contour level $2^x \times 10^y$ e Å^{-5} ($x = 0, 1, 2, 3$; $y = -2, -1, 0, 1, 2, 3$). For all plots the positive values are solid red and the negative values are dashed blue.

Table 3
Multipole refinement details.

F^x	F^{sta}	F^{dyn}	F^{dyn}	F^{sph}	F^{asph}	F^{asph}_{anh}	F^{asph}_{anh}	F^{asph}	F^{asph}
Radial model	sp^3	sp^3	sp^3	sp^3	sp^3	sp^3	sp^3	s^2p^2	s^2p^2
Thermal model	Harmonic	Harmonic	Harmonic, constant $\langle u^2\rangle$	Harmonic	Harmonic	Anharmonic	Harmonic	Harmonic	Harmonic, constant $\langle u^2\rangle$
R_{wp}	N/A	N/A	N/A	0.0293	0.0202	0.0201	0.0201	0.0202	0.0202
RI	N/A	N/A	N/A	0.0374	0.0074	0.0065	0.0065	0.0074	0.0074
RF	0.0019	0.0007	0.0019	0.0033	0.0033	0.0030	0.0033	0.0029	0.0089
RF^2	0.0028	0.0010	0.0026	0.0047	0.0046	0.0043	0.0047	0.0043	0.0120
R_wF	0.0020	0.0008	0.0019	0.0029	0.0026	0.0022	0.0027	0.0024	0.0065
R_wF^2	0.0023	0.0009	0.0019	0.0057	0.0053	0.0045	0.0054	0.0048	0.0131
GoF	N/A	N/A	N/A	0.5895	0.6009	0.5384	0.6121	0.5436	1.4661
Scale	0.9994 (3)	0.9961 (3)	0.9991 (3)	0.984 (1)	1.004 (1)	1.007 (3)	1.016 (1)	1.012 (1)	0.998 (2)
κ'	0.965 (1)	0.9711 (4)	0.965 (1)	0.948 (2)	0.953 (2)	0.966 (3)	0.953 (2)	0.982 (2)	1.005 (3)
κ''	0.853 (4)	0.858 (2)	0.854 (3)	0.881 (7)	0.892 (6)	0.905 (6)	0.894 (7)	0.940 (6)	0.961 (17)
O2−	−0.0141 (2)	−0.0141 (1)	−0.0141 (2)	−0.0155 (4)	−0.0156 (4)	−0.0157 (3)	−0.0156 (4)	−0.0139 (3)	−0.0137 (7)
H0	−0.0056 (3)	−0.0052 (1)	−0.0056 (2)	−0.0063 (8)	−0.0058 (7)	−0.0050 (6)	−0.0057 (7)	−0.0039 (5)	−0.0030 (11)
$\langle u^2\rangle$ (Å^2)	N/A	0.00182 (1)	0.00188	0.00190 (2)	0.00190 (2)	0.00164 (10)	0.00190 (2)	0.00214 (2)	0.00190
c123	N/A	N/A	N/A	N/A	N/A	0.0001 (1)	N/A	N/A	N/A
d1111	N/A	N/A	N/A	N/A	N/A	−0.00060 (21)	N/A	N/A	N/A
d1122	N/A	N/A	N/A	N/A	N/A	−0.00017 (7)	N/A	N/A	N/A
$\Delta\rho_{min}/\Delta\rho_{max}$ (e Å^{-3})	−0.065/0.121	−0.018/0.016	−0.054/0.117	−0.051/0.086	−0.051/0.095	−0.050/0.075	−0.052/0.094	−0.059/0.068	−0.444/0.208

Table 4
Topological details at the C—C bond critical point.

The uncertainties of the topological parameters obtained from the least-squares method are unrealistically low. The uncertainties for these parameters are instead estimated to be at least 0.01 e Å^{-3} for ρ, 0.01 e Å^{-5} for $\nabla^2\rho$ and 0.01 Å for λ.

F^x	F^{sta}	F^{dyn}	F^{dyn}	F^{sph}	F^{asph}	F^{asph}_{anh}	F^{asph}_{anh}	F^{asph}	F^{asph}
Radial model	sp^3	sp^3	sp^3	sp^3	sp^3	sp^3	sp^3	s^2p^2	s^2p^2
Thermal model	Harmonic	Harmonic	Harmonic, constant $\langle u^2\rangle$	Harmonic	Harmonic	Anharmonic	Harmonic	Harmonic	Harmonic, constant $\langle u^2\rangle$
$\rho_{b.c.p.}$ (e Å^{-3})	1.56	1.56	1.56	1.63	1.64	1.64	1.63	1.64	1.63
$\nabla^2\rho_{b.c.p.}$ (e Å^{-5})	−11.97	−11.71	−11.94	−14.84	−14.86	−14.44	−14.81	−13.27	−12.07
λ_1 (Å)	−10.15	−10.20	−10.16	−11.11	−11.26	−11.43	−11.26	−11.39	−11.53
λ_2 (Å)	−10.13	−10.17	−10.14	−11.09	−11.26	−11.43	−11.25	−11.39	−11.52
λ_3 (Å)	8.32	8.66	8.36	7.36	7.65	8.41	7.69	9.51	10.99

seems to be present in the model, which could be due to 'inflexible' κ parameters. This demonstrates that the standard multipole model cannot provide a perfect description of the static electron density in diamond.

Convolution of a thermal parameter of 0.00188 Å^2 on the static density gives a much smoother density, which is better fitted with the multipole model. As can be seen in Table 3 the multipole fit to the dynamic *ab initio* structure factors has a very low residual density ranging from only −0.018 to 0.016 e Å^{-3} (Fig. 5). Like before, the bonding density seems to be described properly, but now the radial deficiency observed in the F^{sta} refinement is no longer present.

Refinement of the thermally convoluted static structure factors (F^{dyn}) should in principle give the exact same refined static electron-density model as refinement of F^{sta}, but as seen in Table 3 the model parameters are not exactly identical and the thermal parameter differs by 3% from the value used in the convolution [0.00182 (1) *versus* 0.00188 Å^2]. The residual factors in the F^{dyn} multipole refinement are much smaller than in the static structure-factor refinement (0.0007 and 0.0010 for RF and RF^2, respectively). It is somehow easier for the multipole model to fit a thermally smeared electron density than a sharp static density. This indicates an insufficient deconvolution of the thermal and electronic contributions to the structure factors even though the resolution of the structure factors is as high as 1.45 Å^{-1}. It is quite surprising that a relatively small change of 3% in the thermal parameter can influence the residual density so much.

The refined multipole electron-density parameters (κ', κ'', O2−, H0) normalized to the values obtained in the refinement of F^{sta} are plotted in Fig. 6 for the different refinements.

Even though small changes are observed for κ' and H0 between the two models (F^{sta} *versus* F^{dyn}), these discrepancies are not significant when compared with the standard uncertainties. As seen in Table 4 small differences in the topological parameters are observed, and $\nabla^2\rho$ and λ_3 have changed from −12.0 e Å^{-3} and 8.32 in the refinement of F^{sta} to −11.7 e Å^{-3} and 8.66 in the F^{dyn} refinement. Figs. 4 and 5 only reveal subtle differences in the deformation densities. The most notable is the small isolated contour next to the carbon nuclei.

If the thermal parameter is fixed at the convoluted value of 0.00188 Å^2 in refinement of F^{dyn}, the refinement results are equivalent to the F^{sta} refinement, and all residual, model and topological parameters are essentially identical (see Fig. 7).

Since the refinement of F^{dyn} with a refinable thermal parameter did not result in exactly the same model as refinement against F^{sta}, it can be concluded that the thermal and electron-density parameters cannot be fully separated in a standard multipole refinement. A small change in the thermal parameter from 0.00188 to 0.00182 Å introduces small changes in the electron-density parameters. Thus, when refining a multipole model even on light atoms one should be aware of the systematic bias in the determined density parameters coming from an imperfect deconvolution of the structure factors into electronic and thermal contributions. The 'poor' multipole fit of the static density leaves question marks. In some sense, thermal motion is the saving grace for the multipole approach to obtaining experimental electron densities. However, since more and more experimental studies are carried out at helium temperature the deficiency in the multipole model will be more and more exposed. Seventeen years ago Figgis *et al.* (1993) noted the multipole radial deficiency in work on copper Tutton salt. In refinement of 85 K data the multipole model performed satisfactorily (Figgis *et al.*, 1992), but when modelling 9 K data it became apparent that more flexible radial functions had to be introduced, and the model was augmented with extra diffuse functions on Cu having 4*s* radial dependence. Recent work by Koritsanszky & Volkov (2004) has focused on a more general improvement of the radial model.

Returning to the experimentally determined structure factors, Table 3 clearly demonstrates that accurate structure factors can be extracted from the synchrotron powder diffraction data. The residual factors *RF*, RF^2 and goodness of fit (GoF) are as low as 0.0033, 0.0047 and 0.5895, respectively, and the residual density interval is from −0.051 to 0.086 e Å^{-3} even when the IAM-extracted structure factors (F^{sph}) are fitted with a multipole model (Fig. 8). This gives strong support to the approach that has been used in the many powder Rietveld/MEM studies in the literature. Here we use the term accurate because the multipole model, even with slight radial deficiency, can be assumed to be close to a true model. Thus, when low residual factors are obtained, the corresponding structure factors must be accurate. In the discussion above the accuracy of the structure factors was probed through comparison with theory, which in that case represented the true model.

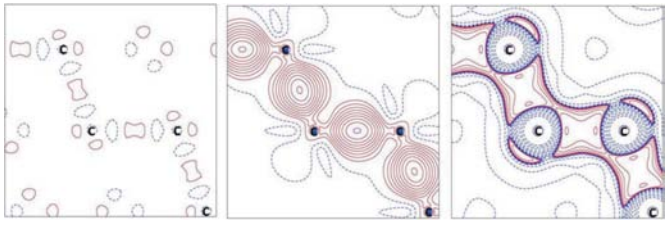

Figure 5
Refinement of F^{dyn}. Left is the residual density with a contour level 0.01 e Å^{-3}, middle is the static deformation density with contour level 0.05 e Å^{-3}, and right is the negative Laplacian with contour level $2^x \times 10^y$ e Å^{-5} (x = 0, 1, 2, 3; y = −2, −1, 0, 1, 2, 3). For all plots the positive values are solid red and the negative values are dashed blue.

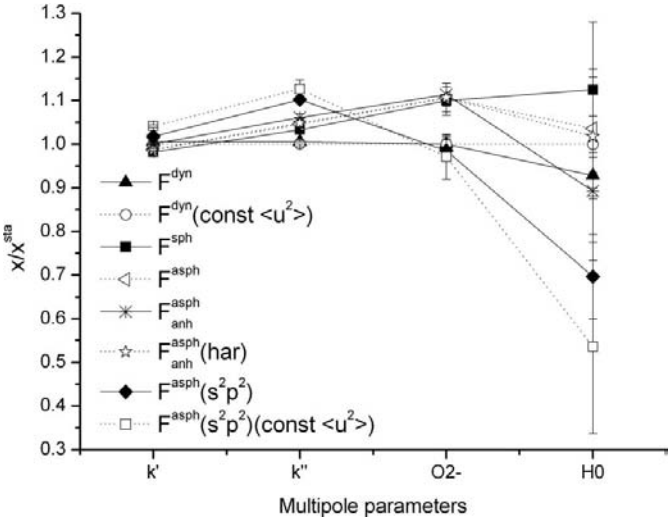

Figure 6
Multipole parameters normalized to the values obtained from refinement of F^{sta}.

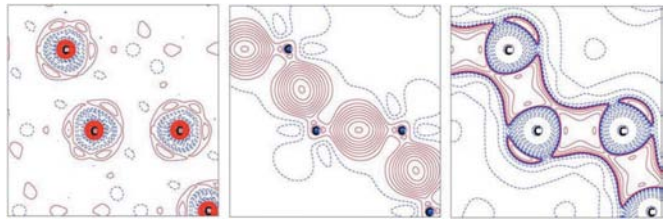

Figure 7
Refinement of F^{dyn} using a constant $\langle u^2 \rangle$ value of 0.00188 Å^2. Left is the residual density with contour level 0.01 e Å^{-3}, middle is the static deformation density with contour level 0.05 e Å^{-3}, and right is the negative Laplacian with contour level $2^x \times 10^y$ e Å^{-5} (x = 0, 1, 2, 3; y = −2, −1, 0, 1, 2, 3). For all plots the positive values are solid red and the negative values are dashed blue.

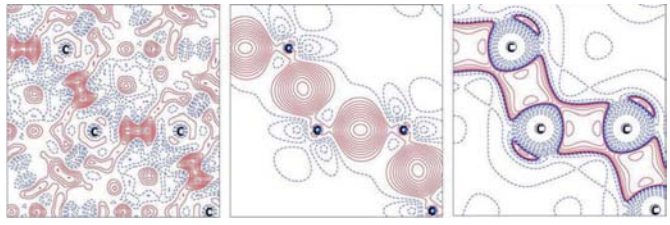

Figure 8
Refinement of F^{sph}. Left is the residual density with contour level 0.01 e Å^{-3}, middle is the static deformation density with contour level 0.05 e Å^{-3}, and right is the negative Laplacian with contour level $2^x \times 10^y$ e Å^{-5} (x = 0, 1, 2, 3; y = −2, −1, 0, 1, 2, 3). For all plots the positive values are solid red and the negative values are dashed blue.

The residual factors and residual density of the refinement of the aspherical extracted structure factors $F^{\rm asph}$ are not improved relative to $F^{\rm sph}$ (RF = 0.0033, RF^2 = 0.0046, GoF = 0.6009, residual density −0.051 to 0.095 e Å^{-3}) (Fig. 9).

Unlike refinements of the theoretical structure factors, residual density is found in the bonding regions. Apparently the multipole model does not fully fit the observed bonding density independently of the choice of extraction model. The refined electron-density parameters (κ', κ'', O2−, H0) from $F^{\rm sph}$ and $F^{\rm asph}$ are almost identical, as seen in Table 3 and Fig. 6. Since the chemical and physical interpretation mainly rests on the static electron-density features, one may therefore argue that in fact the IAM bias in the structure-factor extraction is not significantly affecting the derived multipole model of the density. There is, however, a small but significant change in the refined scale factor between the two refinements ($F^{\rm sph}$ *versus* $F^{\rm asph}$).

The topological parameters obtained from refinement of $F^{\rm sph}$ and $F^{\rm asph}$ are also almost identical, and the density at the bond critical point, $\rho_{\rm b.c.p.}$, only changes from 1.63 e Å^{-3} for $F^{\rm sph}$ to 1.64 e Å^{-3} for $F^{\rm asph}$. With regard to the Laplacian, $\nabla^2\rho_{\rm b.c.p.}$, the values are −14.8 and −14.9 e Å^{-5} for $F^{\rm sph}$ and $F^{\rm asph}$, respectively. However, the individual eigenvalues show some small changes between refinement of $F^{\rm sph}$ and $F^{\rm asph}$. The static deformation densities and Laplacian plots in Figs. 8 and 9 are also very similar. Again, this shows that the effect on the density obtained from introducing multipole division of measured overlapping intensities is not very significant in the present case of crystalline diamond. However, the experimental densities differ slightly from the density obtained from the theoretical static structure factors. Both $\rho_{\rm b.c.p.}$ and especially $\nabla^2\rho_{\rm b.c.p.}$ are different in the model refined against the theoretical structure factors. Even more important is the fact that these differences persist also for the multipole refinement of the dynamic theoretical structure factors. Thus, when comparing the Laplacian and static deformation density plots in Figs. 4 and 5 with Figs. 8 and 9 significant differences are found. The deformation densities obtained from the refinement of the observed structure factors show a larger accumulation of density in the bonding regions and a decrease of density in the region behind the carbon atom. A small negative region is also observed between two bonds, which is not present in the theoretical structure factor refinements. Since the refinements of the observed structure factors in fact have residuals in these regions, the difference between the theoretical and the experimental bonding density is possibly even larger. Thus, even though the multipole model has inadequacies, it is still capable of revealing a distinct difference between the theoretical and the experimental density. This means that the small inter-set R value between $F^{\rm dyn}$ and $F^{\rm asph}$ (= 0.0062) represents a real and measurable difference in the electron density. The present study therefore demonstrates that the level of theory used in this study is not able to reproduce all subtle features in the experimental diffraction data even for a simple system such as crystalline diamond. A further study probing higher levels of theory is necessary in order to investigate whether these differences between experimental and theoretical data persist, but this is beyond the scope of the present work.

When introducing anharmonic thermal displacement parameters in the multipole extraction model and also in the subsequent multipole refinement, the reliability factors slightly decrease to RF = 0.0030, RF^2 = 0.0043 and GoF = 0.5384. The residual density is slightly lower compared with the spherical and aspherical structure-factor refinement using harmonic temperature parameters, −0.050 to 0.075 e Å^{-3} (Fig. 10). Residual density is still present in the bonding regions but in this case it is very oddly oriented – perpendicular to the bonding direction instead of parallel as was observed for the structure-factor refinements using harmonic thermal parameters.

Apparently, a better multipole fit is obtained from the structure factors obtained by including anharmonicity in the extraction, but when comparing the electron-density parameters and thermal parameters with the corresponding values from the refinement of $F^{\rm sta}$ significant differences are observed. As can be seen from Fig. 6, especially the octupole O2− and hexadecapole H0 differ from the static value with changes of 10%. The deformation density shows a slight change in the region behind the carbon atom, and no negative region between two bonds is observed here compared with the refinements of the structure factors extracted using a harmonic temperature factor. Furthermore, the bonding density has become somewhat skewed. The topological para-

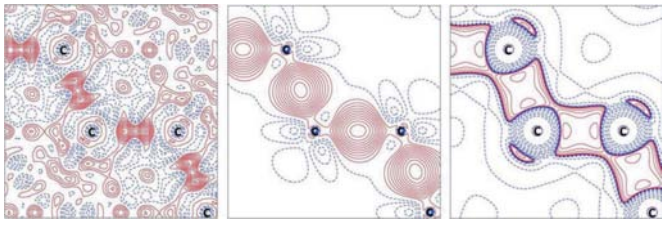

Figure 9
Refinement of $F^{\rm asph}$. Left is the residual density with contour level 0.01 e Å^{-3}, middle is the static deformation density with contour level 0.05 e Å^{-3}, and right is the negative Laplacian with contour level $2^x \times 10^y$ e Å^{-5} (x = 0, 1, 2, 3; y = −2, −1, 0, 1, 2, 3). For all plots the positive values are solid red and the negative values are dashed blue.

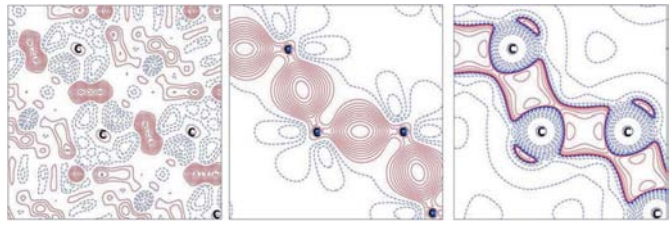

Figure 10
Refinement of $F^{\rm asph}_{\rm anh}$. Left is the residual density with contour level 0.01 e Å^{-3}, middle is the static deformation density with contour level 0.05 e Å^{-3}, and right is the negative Laplacian with contour level $2^x \times 10^y$ e Å^{-5} (x = 0, 1, 2, 3; y = −2, −1, 0, 1, 2, 3). For all plots the positive values are solid red and the negative values are dashed blue.

meters are similar to values obtained from the F^{sph} and F^{asph} refinements. However, the harmonic thermal parameter has decreased very significantly to only 0.00164 Å^2, which is much smaller than the expected value from Fig. 2. The fourth-order Gram–Charlier parameters in the refinement are small but significant. It seems that part of the displacement has been moved from the harmonic parameters to the fourth-order Gram–Charlier parameters, which can be due to the fact that both contributions to the potential are symmetric. A contour plot of the nuclear probability density function (p.d.f.) obtained from the second-order harmonic, as well as third- and fourth-order anharmonic Gram–Charlier components is shown in Fig. 11. A negative region of the p.d.f. is observed in the centre surrounded by a positive region. Such a negative region of the p.d.f. is physically meaningless, and the thermal parameters obtained from the anharmonic refinement do not represent physically realistic atomic motion.

As described earlier anharmonic contributions to the atomic displacement of diamond are not expected at 100 K, and incorporation of 'unphysical' anharmonic parameters apparently merely fits systematic errors in the structure-factor set. By increasing the number of parameters the reliability factors are lowered but at the same time a more unphysical model is obtained and the static density parameters differ significantly from the reference refinement using theoretical static structure factors. It was also previously mentioned that $R(F^{asph}_{anh}, F^{dyn})$ is larger than $R(F^{asph}, F^{dyn})$, indicating a better agreement between the theoretical structure factors and harmonic aspherical extracted structure factors than the corresponding anharmonic aspherical extracted structure-factor sets. Nevertheless, if F^{asph}_{anh} is fitted by a multipole model using a harmonic temperature factor a refined model similar to the F^{asph} refinement model is obtained, as shown in Tables 3 and 4. In this case the thermal parameter has recovered to a value of 0.00190 Å^2.

As a final point we concentrate on the best experimental set of structure factors F^{asph} and probe the accuracy of these experimental structure factors. From general chemical knowledge we expect the carbon atom in diamond to be sp^3 hybridized due to the tetrahedral bonding network. The free carbon atom has an s^2p^2 valence electron configuration. The two configurations have different radial functions, which can be tested against the experimental data. Thus, instead of using the atom Cv from the SCM scattering bank in *XD*, which is a proper sp^3 carbon atom, the normal carbon atom, which is s^2p^2, is used from the same scattering bank. Note that the sp^3 radial dependence of carbon atom Cv is not merely constructed by a different weighting of the *s* and *p* orbitals. As seen in Table 3 the s^2p^2 radial model surprisingly gives a decrease in the refinement residual factors compared with the sp^3 radial model. The residual density, the deformation density and the Laplacian are shown in Fig. 12. However, as in the refinement of F^{asph}_{anh} oddly shaped residual density is present perpendicular to the bonding directions.

The values at the bond critical point are now 1.64 e Å^{-3} and −13.27 e Å^{-5} for $\rho_{b.c.p.}$ and $\nabla^2\rho_{b.c.p.}$, respectively. These topological parameters are actually more similar to the parameters obtained for the theoretical structure factor refinements, and the residual factors and density are also lower compared to the corresponding experimental sp^3 model values. However, one of the major changes between the s^2p^2

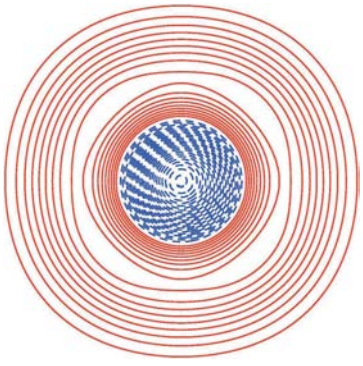

Figure 11
Plot of the nuclear probability density function obtained from the second-order harmonic and third- and fourth-order anharmonic Gram–Charlier components with contour level 2000 Å^{-3}. The positive values are solid red and the negative values are dashed blue.

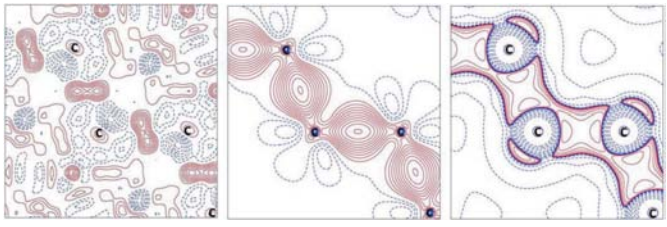

Figure 12
Refinement of F^{asph} using an s^2p^2 radial model. Left is the residual density with contour level 0.01 e Å^{-3}, middle is the static deformation density with contour level 0.05 e Å^{-3}, and right is the negative Laplacian with contour level $2^x \times 10^y$ e Å^{-5} (x = 0, 1, 2, 3; y = −2, −1, 0, 1, 2, 3). For all plots the positive values are solid red and the negative values are dashed blue.

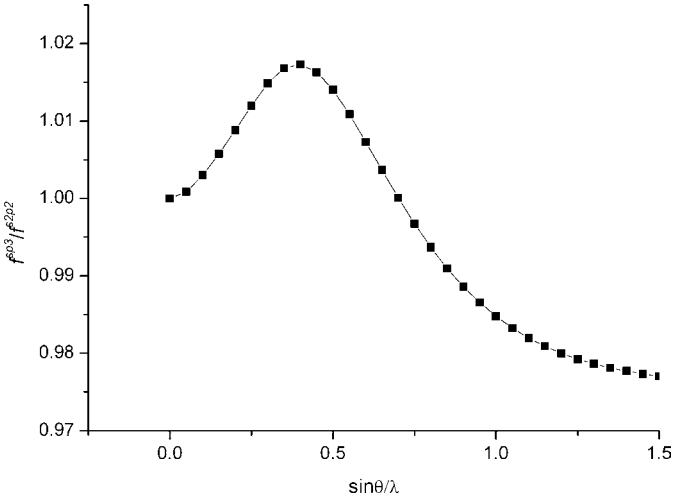

Figure 13
Plot of the ratio between the total radial scattering factors for sp^3 (f^{sp^3}) and s^2p^2 ($f^{s^2p^2}$) carbon atoms as a function of sin θ/λ.

Table 5
Correlations between the different refined parameters listed in pairs for the refinement of F^{asph} using the s^2p^2 and sp^3 radial models.

	Correlation (%) s^2p^2	Correlation (%) sp^3
Scale κ'	66	70
Scale $\langle u^2\rangle$	87	88
$\langle u^2\rangle$ κ'	56	60
κ'–κ''	68	69
κ''–H0	63	70
κ'–H0	64	70
H0–O2−	51	63

and sp^3 models is the thermal parameter, which has increased to the unphysical value of 0.00214 (2) Å^2 in the s^2p^2 model. This value is too large, since the Wilson plot in Fig. 2 resulted in an isotropic thermal parameter value of 0.00188 (2) Å^2. This increase in the thermal parameter can be explained by exploring the difference between the s^2p^2 and sp^3 radial scattering functions. In Fig. 13 the ratio between the total radial scattering factors for sp^3 (f^{sp3}) and s^2p^2 (f^{s2p2}) carbon atoms is plotted. The plot illustrates that the radial scattering curves for s^2p^2 and sp^3 carbon atoms cannot be superimposed merely by a scale factor, and a κ refinement alone will not be able to absorb the difference. At high angles the ratio between the radial scattering factors is smaller than 1, indicating larger density near the core in the s^2p^2 model compared with the sp^3 model. In order to compensate for this difference the refined s^2p^2 model has an increased thermal parameter. At the same time the low-angle region yields a ratio greater than 1 due to a more diffuse s^2p^2 valence density. Hence, a contraction of the valence density by increasing κ' is observed in the s^2p^2 model refinement.

Thus, the multipole model remedies the radial defectiveness in the s^2p^2 electron-density model with a combination of changes in κ' and the thermal parameter. From Fig. 6 it is also clear that the other electron-density parameters differ strongly from the F^{sta} refinement values, and in fact the hexadecapole H0, for example, differs by 30%. This is again a concrete example of the correlation between electron density and thermal parameters. Thus, even though the data set extends to high resolution (1.45 Å^{-1}) in a light-atom structure, and the thermal parameters presumably should be 'determined' from the refinement of the high-order data, which contain 'no' valence-electron-density information, the multipole model with an inappropriate radial model comes out with a clearly biased thermal parameter. This illustrates the limitation in the commonly used high-order refinement to obtain presumably unbiased thermal parameters, and it also underlines the importance of using good radial functions in accurate charge-density studies. In Table 5 we list explicitly the correlation coefficients from the refinements using the two different radial scattering factors. The scale factor, the thermal parameter and the κ parameters indeed have substantial correlation for both models.

If we do not allow the s^2p^2 multipole model to 'remedy' the radial defectiveness with the thermal parameter, *i.e.* we fix the thermal parameters at the value obtained from refinement of F^{asph} (0.00190 Å^2), the resulting residual parameters and R values increase enormously to −0.444–0.208 e Å^{-3}, and RF, RF^2 and GoF are now as high as 0.0089, 0.0120 and 1.4661, respectively (Fig. 14). Furthermore, the electron-density parameters differ even more from the static values as seen in Fig. 6, and the shapes of the bonding density as well as the carbon density have changed significantly. Thus, the presumably quite subtle error in the radial function, which supposedly should just be remedied by the κ refinement, in fact causes a significant change in the derived electron density.

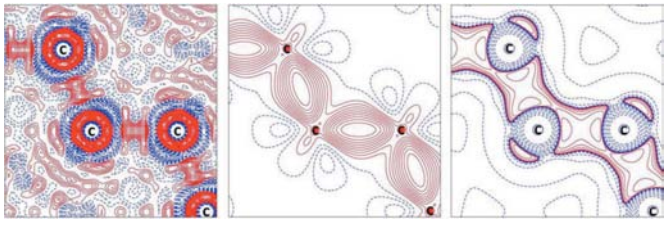

Figure 14
Refinement of F^{asph} using an s^2p^2 radial model and a fixed $\langle u^2\rangle$ value of 0.00190 Å^2. Left is the residual density with contour level 0.01 e Å^{-3}, middle is the static deformation density with contour level 0.05 e Å^{-3}, and right is the negative Laplacian with contour level $2^x \times 10^y$ e Å^{-5} (x = 0, 1, 2, 3; y = −2, −1, 0, 1, 2, 3). For all plots the positive values are solid red and the negative values are dashed blue.

4. Conclusion

In the present paper we have shown that accurate structure factors of diamond can be extracted from powder diffraction data even using a spherical IAM model. Introducing multipoles in the extraction did not significantly improve the quality of the observed structure factors for crystalline diamond. The bonds are highly covalent in diamond, and the valence electrons dominate in the low-angle region. Since only limited peak overlap is present in this region, the extraction of the structure factors for diamond is almost independent of the choice of density model used for extracting observed structure factors. Hence, the aspherical bonding features are still included in the structure factors even if an IAM model is used in the extraction. However, if more complicated structures are investigated, where significant peak overlap is present also at low order, the present extraction based on the multipole model must be expected to improve the accuracy of the observed structure factors. Overall, the F^{asph} structure-factor set therefore must be regarded as the most accurate set in the present study.

Introduction of anharmonicity in the model used for structure-factor extraction leads to significant changes in the structure-factor values, since these parameters affect the high-order region where peak overlap is significant. Since diamond has extremely small thermal expansion, the introduction of such parameters is 'unphysical'. The corresponding multipole model has large unphysical changes in the ADP and an odd-looking residual density.

If a slightly wrong radial model is used in the multipole refinement (s^2p^2 instead sp^3), the radial defectiveness leads to a wrong thermal parameter. The slight change in the radial scattering factor cannot be adequately modelled by refinement of κ parameters. This shows the clear correlation between electron density and thermal parameters even for a light atom such as carbon. Fixing the thermal parameter to the correct value leads to a relatively poor representation of the static electron density. The analysis exposes the limitations in the commonly used 'high-order' refinement to obtain presumably unbiased ADPs.

Overall a good agreement was found between the observed structure factors obtained from synchrotron powder diffraction and the theoretical structure factors derived from *ab initio* theory. If theory is assumed to be close to the true density, it can be concluded that accurate structure factors can be extracted from synchrotron powder diffraction data. Nevertheless, the small inter-set R value between $F^{\rm dyn}$ and $F^{\rm asph}$ (0.0062) does lead to subtle differences in the multipole refined densities. Even though the effect is small, the present data suggest that the level of theory used in this study is not able to reproduce all features in the experimental data even for a simple structure such as crystalline diamond. In order to determine whether these differences between experimental and theoretical data are important it is necessary to carry out further studies probing higher levels of theory.

The study was supported by the Danish National Research Foundation and by the Japanese Ministry of Education, Culture, Sports, Science and Technology, Grant-in-Aid for Scientific Research (B), 20360006, and Young Scientists (A), 17686003.

References

Alkire, R. W., Yelon, W. B. & Schneider, J. R. (1982). *Phys. Rev. B*, **26**, 3097–3104.

Ashcroft, N. W. & Mermin, N. D. (1976). *Solid State Physics*. London: Thomson Learning, Inc.

Blöchl, P. E. (1994). *Phys. Rev. B*, **50**, 17953–17979.

Bolotovsky, R., Darovsky, A., Kezerashvili, V. & Coppens, P. (1995). *J. Synchrotron Rad.* **2**, 181–184.

Cargnoni, F., Nishibori, E., Rabiller, P., Bertini, L., Snyder, G. J., Christensen, M., Gatti, C. & Iversen, B. B. (2004). *Chem. Eur. J.* **10**, 3861–3870.

Clausen, H. F., Overgaard, J., Chen, Y. S. & Iversen, B. B. (2008). *J. Am. Chem. Soc.* **130**, 7988–7996.

Coppens, P. (1997). *X-ray Charge Densities and Chemical Bonding*. Oxford University Press.

Coppens, P., Iversen, B. B. & Larsen, F. K. (2005). *Coord. Chem. Rev.* **249**, 179–195.

Dawson, B. (1967). *Proc. R. Soc. London Ser. A*, **298**, 264–288.

Dawson, B. & Sanger, P. L. (1967). *Proc. R. Soc. London Ser. A*, **301**, 195–209.

Figgis, B. N., Iversen, B. B., Larson, F. K. & Reynolds, P. A. (1993). *Acta Cryst.* B**49**, 794–806.

Figgis, B. N., Khor, L., Kucharski, E. S. & Reynolds, P. A. (1992). *Acta Cryst.* B**48**, 144–151.

Flensburg, C. & Stewart, R. F. (1999). *Phys. Rev. B*, **60**, 284–291.

Göttlicher, S. & Wölfel, E. (1959). *Z. Elektrochem.* **63**, 891–901.

Hansen, N. K. & Coppens, P. (1978). *Acta Cryst.* A**34**, 909–921.

Harel, M., Hecht, M. & Hirshfeld, F. L. (1975). *Acta Cryst.* B**31**, s224.

Hofmann, A., Kalinowski, R., Luger, P. & van Smaalen, S. (2007). *Acta Cryst.* B**63**, 633–643.

Iversen, B. B., Larsen, F. K., Figgis, B. N., Reynolds, P. A. & Schultz, A. J. (1996). *Acta Cryst.* B**52**, 923–931.

Iversen, B. B., Larsen, F. K., Pinkerton, A. A., Martin, A., Darovsky, A. & Reynolds, P. A. (1999). *Acta Cryst.* B**55**, 363–374.

Iversen, B. B., Larsen, F. K., Souhassou, M. & Takata, M. (1995). *Acta Cryst.* B**51**, 580–591.

Kitaura, R., Kitagawa, S., Kubota, Y., Kobayashi, T. C., Kindo, K., Mita, Y., Matsuo, A., Kobayashi, M., Chang, H., Ozawa, T. C., Suzuki, M., Sakata, M. & Takata, M. (2002). *Science*, **298**, 2358–2361.

Koritsansky, T. & Coppens, P. (2001). *Chem. Rev.* **101**, 1583–1627.

Koritsanszky, T., Flaig, R., Zobel, D., Krane, H.-G., Morgenroth, W. & Luger, P. (1998). *Science*, **279**, 356–358.

Koritsanszky, T. & Volkov, A. (2004). *Chem. Phys. Lett.* **385**, 431–434.

Kumazawa, S., Kubota, Y., Takata, M., Sakata, M. & Ishibashi, Y. (1993). *J. Appl. Cryst.* **26**, 453–457.

Kurki-Suonio, K. & Ruuskanen, A. (1971). *Ann. Acad. Sci. Fenn. Ser. A6*, **358**, 1–28.

Macchi, P. & Coppens, P. (2001). *Acta Cryst.* A**57**, 656–662.

McConnell, J. F. & Sanger, P. L. (1970). *Acta Cryst.* A**26**, 83–93.

Morgenroth, W., Overgaard, J., Clausen, H. F., Svendsen, H., Jørgensen, M. R. V., Larsen, F. K. & Iversen, B. B. (2008). *J. Appl. Cryst.* **41**, 846–853.

Nishibori, E., Sunaoshi, E., Yoshida, A., Aoyagi, S., Kato, K., Takata, M. & Sakata, M. (2007). *Acta Cryst.* A**63**, 43–52.

Overgaard, J., Iversen, B. B., Palii, S., Timco, G. A., Gerbeleu, N. V. & Larsen, F. K. (2002). *Chem. Eur. J.* **8**, 2775–2786.

Overgaard, J., Larsen, F. K., Schiøtt, B. & Iversen, B. B. (2003). *J. Am. Chem. Soc.* **125**, 11088–11099.

Overgaard, J., Schiøtt, B., Larsen, F. K. & Iversen, B. B. (2001). *Chem. Eur. J.* **7**, 3756–3767.

Perdew, J. P., Burke, K. & Ernzerhof, M. (1996). *Phys. Rev. Lett.* **77**, 3865–3868.

Poulsen, R. D., Bentien, A., Chevalier, M. A. & Iversen, B. B. (2005). *J. Am. Chem. Soc.* **127**, 9156–9166.

Price, P. F. & Maslen, E. N. (1978). *Acta Cryst.* A**34**, 173–183.

Roversi, P., Irwin, J. J. & Bricogne, G. (1998). *Acta Cryst.* A**54**, 971–996.

Sakata, M. & Sato, M. (1990). *Acta Cryst.* A**46**, 263–270.

Schwarz, W. H. E. (2006). *Angew. Chem. Int. Ed.* **45**, 1508–1517.

Smaalen, S. van & Netzel, J. (2009). *Phys. Scr.* **79**, 048304.

Spackman, M. A. (1991). *Acta Cryst.* A**47**, 420–427.

Stewart, R. F. (1973*a*). *J. Chem. Phys.* **58**, 4430–4438.

Stewart, R. F. (1973*b*). *Acta Cryst.* A**29**, 602–605.

Stewart, R. F. (1976). *Acta Cryst.* A**32**, 565–574.

Su, Z. & Coppens, P. (1998). *Acta Cryst.* A**54**, 646–652.

Takama, T., Tsuchiya, K., Kobayashi, K. & Sato, S. (1990). *Acta Cryst.* A**46**, 514–517.

Takata, M., Nishibori, E. & Sakata, M. (2001). *Z. Kristallogr.* **216**, 71–86.

Takata, M., Umeda, B., Nishibori, E., Sakata, M., Saito, Y., Ohno, M. & Shinohara, H. (1995). *Nature* (*London*), **377**, 46–49.

Tischler, J. Z. & Batterman, B. W. (1984). *Phys. Rev. B*, **30**, 7060–7066.

Trucano, P. & Batterman, B. W. (1972). *Phys. Rev. B*, **6**, 3659–3666.

Tsirelson, V. & Ozerov, R. R. (1996). *Electron Density and Bonding in Crystals: Principles, Theory and X-ray Diffraction Experiments in Solid State Physics and Chemistry*. Bristol, Philadelphia: Institute of Physics Publishing.

Volkov, A., Macchi, P., Farrugia, L., Gatti, C., Mallinson, P., Richter, T. & Koritzansky, T. (2006). *XD2006. A Computer*

Program Package for Mulitpole Refinement, Topological Analysis of Charge Densities and Evaluation of Intermolecular Energies from Experimental and Theoretical Structure Factors. University at Buffalo, State University of New York, USA; University of Milan, Italy; University of Glasgow, UK; CNRISTM, Milan, Italy; and Middle Tennessee State University, USA.

Wang, S. G. & Schwarz, W. H. E. (2000). *Angew. Chem. Int. Ed.* **39**, 1757–1762.

Weiss, R. J. (1964). *Phys. Lett.* **12**, 293–295.

Yamamoto, K., Takahashi, Y., Ohshima, K., Okamura, F. P. & Yukino, K. (1996). *Acta Cryst.* A**52**, 606–613.

Zuo, J. M., Kim, M., O'Keeffe, M. & Spence, J. C. H. (1999). *Nature* (*London*), **401**, 49–52.